Platypus — Indoor Localization and Identification through Sensing Electric Potential Changes in Human Bodies

Tobias Grosse-Puppendahl[1], Xavier Dellangnol[2], Christian Hatzfeld[2], Biying Fu[3], Mario Kupnik[2], Arjan Kuijper[2,3], Matthias R. Hastall[4], James Scott[1], Marco Gruteser[5]
[1]Microsoft Research, 21 Station Road, CB1 2FB Cambridge, UK,
{tgp,jws}@microsoft.com
[2]Technische Universität Darmstadt, Karolinenplatz 5, 64283 Darmstadt, Germany,
xdell@live.fr, {c.hatzfeld,kupnik}@emk.tu-darmstadt.de
[3]Fraunhofer IGD, Fraunhoferstr. 5, 64283 Darmstadt, Germany,
{biying.fu,arjan.kuijper}@igd.fraunhofer.de
[4]TU Dortmund University, Emil-Figge-Str. 50, 44227 Dortmund, Germany,
matthias.hastall@tu-dortmund.de
[5]WINLAB, Rutgers University, New Jersey 08902, USA,
gruteser@winlab.rutgers.edu

ABSTRACT

Platypus is the first system to localize and identify people by remotely and passively sensing changes in their body electric potential which occur naturally during walking. While it uses three or more electric potential sensors with a maximum range of 2 m, as a tag-free system it does not require the user to carry any special hardware. We describe the physical principles behind body electric potential changes, and a predictive mathematical model of how this affects a passive electric field sensor. By inverting this model and combining data from sensors, we infer a method for localizing people and experimentally demonstrate a median localization error of 0.16 m. We also use the model to remotely infer the change in body electric potential with a mean error of 8.8 % compared to direct contact-based measurements. We show how the reconstructed body electric potential differs from person to person and thereby how to perform identification. Based on short walking sequences of 5 s, we identify four users with an accuracy of 94 %, and 30 users with an accuracy of 75 %. We demonstrate that identification features are valid over multiple days, though change with footwear.

Categories and Subject Descriptors

H.5.m [**Information Interfaces and Presentation (I.7)**]: Miscellaneous

Keywords

localization; identification; capacitive sensing; electric potential sensing

MobiSys '16, June 25–30, 2016, Singapore.

DOI: http://dx.doi.org/10.1145/2906388.2906402

1. INTRODUCTION

Localizing and identifying humans in indoor spaces has been a challenging problem in mobile and pervasive computing for many years [56, 39, 32]. Applications in valuable domains like home automation [30], institutional care [60], and personalized energy metering [64] rely on localization and identification information.

Ideally, such a system should be "tag free", so that the users at home or in an office environment are not required to carry any particular hardware. Existing tag-free approaches have relied on sensing various properties of humans such as sounds they make [22], heat emissions [42] or the effect of the body on RF signals [1, 36]. In our system we remotely sense a different underlying quantity: the electric potential carried by the human body. Unlike existing capacitive sensing systems that actively generate an electric field to sense people [57, 9], we passively *observe* naturally occurring electric field changes, similarly to platypuses when hunting underwater preys [16].

As people move, their bodies' electric potential changes when interacting with the environment. The most significant changes occur through two means: static charging explained by the triboelectric effect [10], and changes in capacitive coupling to the environment as one's feet move towards and away from the floor during walking [17]. With Platypus, we remotely infer body electric potential changes at distances up to 2 m using a distributed grid of passive electric field sensors. Requiring at least three sensors, we have developed a method of inferring both the location of the body and the characteristic signature pattern of electric potential changes that occurs when walking, which permits identification of users.

The contribution of this paper is the introduction of Platypus, a novel use of electric field sensing that supports both localization and user differentiation:

- We localize a person observing the ambient electric field, further reconstruct body electric potential change, and extract a signature for identification.

- We detail the physical principles behind Platypus, the mathematical models and working prototype hardware.
- Based on detailed experiments, we show that Platypus achieves a median localization error of 16 cm for a walking user.
- We experimentally validate Platypus's ability to recognize users based on their signature of electric potential changes during walking; we observe an average accuracy of 94 % for 4 users and 75 % for 30 users.

2. BACKGROUND & RELATED WORK

2.1 Localization & Identification Systems

Indoor localization and identification systems can be divided into *tag-dependent* and *tag-free* [32, 35, 39, 56]. Tag-free systems, including Platypus, do not limit who is monitored to those with tags, or require specific behaviour (carrying the tag). We therefore focus on other tag-free systems as comparisons for Platypus.

Camera-based systems [60], including depth [62] cameras, can localize people accurately (error < 1 cm) as well as identify them with face and/or body shape recognition. However, privacy and security concerns make them unsuitable for some environments [31]. Similar concerns may be raised when using an array of microphones to recognize human activities (e.g. talking or opening a door). These can be realized with techniques such as time difference of arrival [7] and may also require classification of sounds [22].

Infrared sensors have been used as binary [52] as well as analog [26, 41, 42] sources for localization. The modality is a low-power, low-cost solution [42] that can even track multiple targets [63], and potentially perform identification by gait analysis [65]. Pressure-sensitive or capacitive localization systems use sensors deployed underneath the floor or integrated in furniture [8, 9, 51, 57]. The effort of installing such systems is large, as changes to existing flooring are required [9].

Various RF-based tag-free localization methods have been presented, using ultra-wideband radar [48], radio tomography [61], RSSI fingerprinting [2], WiFi Doppler [47] and FMCW-modulated radar [1]. Recent systems have leveraged Wi-Fi for vital sign detection [36] or to recognize spoken words [58].

Identification and room-level localization has been demonstrated by ultrasonic distance sensors used to measure the height of occupants, e.g. as they walk through doors [28, 54]. Compared to these weak biometric factors related to body height and movements, we investigate an even more temporary factor that changes with footwear and clothing. This can be regarded as a privacy advantage, allowing to identify a person for as long as the same shoes are worn.

Our system Platypus uses changes in body electric potential due to walking, which is a different underlying physical mechanism to any above. This modality has a particular set of trade-offs. It is passive, requiring no injection of e.g. RF or audio into the environment. Like PIR, camera and audio systems, it cannot operate through walls, in contrast to RF systems [47]. While active capacitive techniques are susceptible to high-frequency noise, Platypus as a passive system has a cut-off frequency of less than 10 Hz. Higher frequency components, e.g. injected by power-lines [15] or switch-mode power supplies [34], have a limited effect on the operation of Platypus. Other appliances like fluorescent lamps, gas ovens, and electro-magnetic motors emit lower frequency electric fields that can inject noise [34].

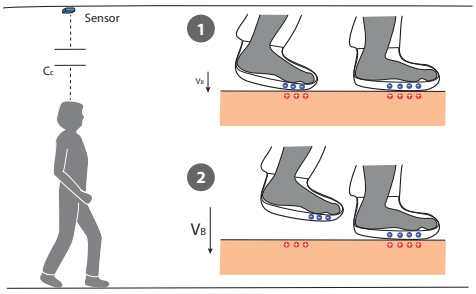

Figure 1: Platypus uses a passive electric field sensor to sense changes in a body electric potential due to (1) triboelectric charging, and (2) capacitance changes.

Passive electric field sensing has been used to measure body electric potential in body-attached [14, 49] as well as stationary applications [13, 45]. Cohn et al. investigated the technique as a low-power replacement for accelerometers by measuring the body electric potential with a wrist-worn node. The approach allows for motion recognition, and similar to Rekimoto et al. [49], enables the sensing of footsteps which induce a large change in body electric potential. Stationary approaches include sensing of electric potential changes through step variations [33]. Different to sensing the body electric potential, the capacitive coupling to the environment can be measured with active techniques, as shown by Haescher et al. [23].

2.2 Electric Potential of the Human Body

Every object in our environment carries electric charge, which gives rise to differences in electric potential between objects. Considering humans, changes in electric potential occur internally, caused by heartbeats or muscle movements, or body-wide changes, for example when walking. With Platypus, we focus on sensing the body-wide change in human body electric potential. While walking with shoes, two physical phenomena cause the most variation in the body electric potential: changes in charge explained by the triboelectric effect and capacitance variations (see Figure 1).

As a shoe comes into contact with the ground, the soles and the flooring material become charged through contact. This effect, known as triboelectric effect, is a matter of common experience, such as rubbing one's hair with a balloon [29, 38, 50]. Recombination and leaking phenomena, such as current circulating through the soles, oppose the accumulation of charge Q, leading to a saturation effect [17]. When walking, the capacitive coupling C between body and grounded objects in the environment changes, mostly due to the variations in distance between the sole of the foot and the floor. When the person lifts a foot, this distance is raised, the capacitive coupling to ground decreases, and the body electric potential V increases since $V = Q/C$. The inverse happens when the foot is put back down. A regular walking motion therefore results in a periodic variation of body electric potential [17] (Figure 3).

2.3 Measuring Ambient Electric Potentials

Low-frequency electric fields can be measured with various devices, for instance field mills [4], electro-optic sensors [27]

Figure 2: Custom sensor board, integrating an electric potential sensor from Plessey Semiconductors [44].

or induction probes [37]. The latter are the simplest to build and use outside of a laboratory [5]. A basic induction probe consists of an amplifier connected to an electrode on which the ambient electric field induces a weak charge. The electrode eventually discharges through the amplifier's finite input impedance, which makes this apparatus unable to measure static electric fields. Rekimoto [49] and Kurita [33] built their own induction probes to sense the influence of human activity on the ambient electric field. Due to the passive approach and the low operating frequencies, EPS were realized with a power consumption of $6.6\,\mu W$ [14]. A similar sensor with very large input impedance (about $10^{15}\,\Omega$), large bandwidth (mHz to MHz) and low noise [5] was designed at the University of Sussex [13, 19, 25]. This device is known as an *electric potential sensor* (EPS) and commercially available under the name *electric potential integrated circuit* (EPIC) [44].

3. SYSTEM OVERVIEW

Platypus exploits natural changes in human body electric potential to provide localization and identification. It relies on electric potential sensors attached high on walls or on ceilings that are sensitive enough to be used up to 2 m to a person. A minimum of three sensors allows us to estimate the position of a person and, based on this information, the change in body electric potential occurring when stepping. In typical installations however, we use two rectangular cells composed of six sensors to increase performance. The body electric potential exhibits a characteristic pattern enabling us to distinguish people from each other, using a movement sequence of approximately 5 s.

We integrated a Plessey EPIC sensor [44] on a custom peripheral board (Figure 2) to measure the ambient electric potential. The board provides a bipolar power supply as well as an operational amplifier (OPA2322) for voltage level translation (33 mW total power consumption per sensor). We connect an array of up to six sensors to an OpenCapSense board [20], which conducts 50 analog-to-digital conversions each second, and performs digital filtering to remove mains hum.

Figure 3 (bottom) depicts a walking activity underneath four sensors attached to the ceiling in a rectangular configuration. The amplitude of a sensor signal increases when the person moves closer to the sensor (e.g. sensor 4) and vice versa. Two other important effects play into this measurement, however: (1) the charge carried on the body and (2) the change in coupling to the environment. Using an EPS, we are not able to distinguish between these two effects and we base our observations on the combination of both: the body electric potential. This can be observed in Figure 3 (top), which shows a direct body voltage measurement from a voltmeter attached to a walking person. It can be seen that the charge carried on the body increases slowly to a saturation point (effect 1). The steps taken by a person

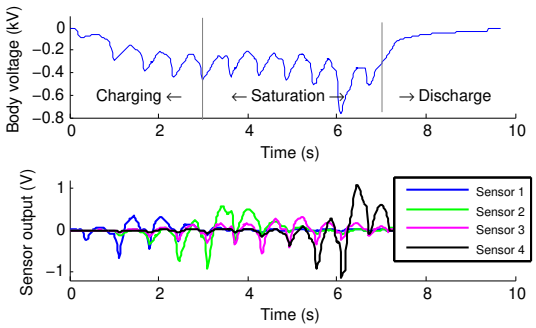

Figure 3: The top plot represents a contact-based measurement of absolute body electric potential. When walking, the potential gradually increases up to a saturation point, while exhibiting peaks when a foot is lifted. An array of four sensors (bottom) detects these changes, with highest amplitude as the walker passes under them.

influence the environmental coupling and lead to recurring peaks (effect 2). When the person stops walking, the charge decreases within a couple of seconds.

In order to make meaningful assumptions about a person's position and change in body electric potential, it is necessary to describe them based on the physical principles of the sensing modality. We do so by introducing a model that predicts how sensor values change when a human affects the ambient electric field. By inverting the model, we can derive a person's position from a set of real sensor readings. Once this position is known, the change in body electric potential can be reconstructed. We show that this change is specific for a person, and that it can leverage identification using an SVM classifier with a feature set extracted from a short walking sequence (typ. 5 s).

4. MODELING THE SENSOR RESPONSE

We now derive a forward (or predictive) model that estimates sensor values based on a person's location and body electric potential. This forward model enables us to understand how human movements are reflected in our sensor signals. The model also acts as a means to validate our assumptions on reconstructing body electric potential and localization by matching model predictions with experimental data. Let us first consider the dynamic sensor response to a changing input.

An EPS can be modelled using a resistor and a capacitor, in combination with an ideal voltage follower, as shown in the right part of Figure 4 [13]. Recall that a voltage follower is an amplifier with a gain of 1, it simply follows the voltage at its input, which is connected to the sensing electrode. By using the amplifier, the electrode is decoupled from the sensing circuit, enabling it to adapt to changes in the ambient electric field.

The voltage follower's output is v_S. Its input capacitance and resistance are explicitly represented by C_{in} and R_{in}, respectively. As for the electric field generated by a human body, it is equivalent to a voltage source v_B coupled to the sensor through a very small capacitance C_C, usually less than 100 fF. In human movement sensing applications, the distance between the person and the sensor is typically in the meter range, which results in a weak coupling ($C_C \ll C_{in}$) [45].

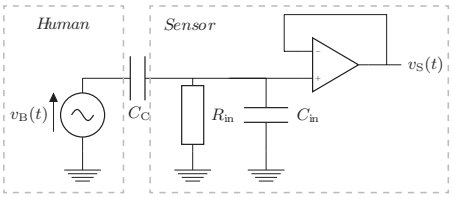

Figure 4: Electric potential sensor represented by an equivalent circuit (adapted from [13]). v_b represents the changing body electric potential, whereas C_C is the coupling capacitance which changes with the body-to-sensor distance.

When the person moves relatively to the EPS, C_C is not a constant but depends on the body-to-sensor distance d. In order to simplify the notation, d is considered a function of time $d(t)$ in the following, and the coupling capacitance is written $C_C(t)$. Analyzing the circuit yields

$$v_S{}'(t)[C_C(t) + C_{in}] + v_S(t)[C_C{}'(t) + 1/R_{in}] = \frac{d}{dt}[C_C(t)v_B(t)] \,. \quad (1)$$

We can solve (1) for the sensor output v_S by assuming that $C_C(t) \ll C_{in}$ and $C_C{}'(t) \ll 1/R_{in}$ for all t. These assumptions are justified in weak coupling situations with a high input impedance sensor such as the EPIC. Additionally, we introduce a first-order low-pass filter with impulse response $h_1(t)$ (time constant $\tau_1 = R_{in}C_{in}$), and a first-order high-pass filter with impulse response $h_2(t)$ (cutoff frequency typically in the mHz range). The first filter simplifies the expression, and the second models the effect of the passive components integrated in the EPS [46]. The output of an EPS is finally

$$v_S(t) = R_{in}h_1(t) * h_2(t) * \left(\frac{d}{dt}[C_C(t)v_B(t)]\right) \,. \quad (2)$$

With this equation, we are able to predict a sensor output based on the two variables of coupling capacitance and body voltage.

4.1 Coupling Capacitances

We now take a closer look on how coupling capacitances are related to a person's distance to a sensor. To derive the coupling capacitance C_C, we start with a point charge approximation [11], in which $C_C(d) \propto 1/d^2$. We generalize this slightly to $C_C(d) \propto 1/d^\alpha$ where a constant α is the distance exponent, to account for deviations from the point charge approximation [53, 21]. In the far field/weak coupling case, there must be a lower limit d_{min} to the distance corresponding to an upper limit $C_{C,max}$ to the coupling capacitance, so that

$$C_C(d) = C_{C,max}\left(\frac{d_{min}}{d}\right)^\alpha \,. \quad (3)$$

Placing the sensors on a room's ceiling (or at the top of walls) ensures that there is a minimum distance of about 0.5 m to 1 m between the ceiling and the top of the person's head. This point approximates the participant's position, assuming the human body is perfectly conducting at low frequencies [18]. With an electrode of about 1 cm^2, the point charge approximation is justified, at least on the sensor side. Knowing that the sensors are on the ceiling, the constant minimum height between the top of the person's head and the sensors is defined as

$$H = \text{ceiling height} - \text{person's height}. \quad (4)$$

We introduce the simplification that the coordinates of a person may only vary in two dimensions. Let $(x(t), y(t), z(t))$ be the person's coordinates at time t, and (x_S, y_S, z_S) the coordinates of a sensor. The $z = 0$ plane is the space where the top of the person's head moves. This allows to write the Euclidean distance between the head and the sensor, and define the minimum distance $d_{min} = H$. The final coupling capacitance is

$$C_C(t) = \frac{C_{C,max}H^\alpha}{\left([x(t) - x_S]^2 + [y(t) - y_S]^2 + H^2\right)^{\alpha/2}} \,. \quad (5)$$

4.2 Complete Forward Model

We described models for the EPIC sensor (2) and the body to sensor coupling (5). Each element of the measurement situation (Figure 1) is known. Let us synthesize this knowledge in a complete forward model.

For further derivations, it will be useful to separate the filters' responses in (2) from the rest of the expression. The filtered signal is the derivative of a product, that may be expressed as a sum thanks to the product rule. The two elements of this sum are

$$\Psi_a(t) = R_{in}C_C(t)v_B{}'(t), \text{ and} \quad (6)$$

$$\Psi_b(t) = R_{in}C_C{}'(t)v_B(t) \,. \quad (7)$$

With the coupling capacitance (5), the expressions of $\Psi_a(t)$ (6) and $\Psi_b(t)$ (7) can be inferred. Let us focus on Ψ_a, which is related to the change in body electric potential, for example caused by stepping:

$$\Psi_a(t) = \frac{R_{in}C_{C,max}H^\alpha v_B{}'(t)}{\left([x(t) - x_S]^2 + [y(t) - y_S]^2 + H^2\right)^{\alpha/2}} \,. \quad (8)$$

The signals that compose the response of an EPIC are filtered versions of Ψ_a and Ψ_b, which is noted $\psi_a(t) = h_1(t) * h_2(t) * \Psi_a(t)$ and $\psi_b(t) = h_1(t) * h_2(t) * \Psi_b(t)$.

To complete the forward model, an experimental phenomenon is considered: the sensor placement within the room influences the amplitude of the output. For instance, an EPS has a strong coupling to the environment when placed close to a wall. If this coupling increases the circuit's input impedance, the amplitude of the sensor output is decreased. Let this effect be approximated by a simple dimensionless factor, the *calibration constant* K. Including the partial components ψ_a, ψ_b and the calibration constant, the expression

$$v_S(t) = K\left[\psi_a(t) + \psi_b(t)\right] \,. \quad (9)$$

describes the output of an EPIC, depending on the body's position and electric potential.

The measurement result is a filtered combination of the body electric potential, its derivative, the position and the speed. This is a new formulation of an old observation. As Aronoff et al. [3] already noted in 1965, the variable electric field generated by a walking human being is a combination of two effects: the variable electric potential (due to stepping) of a static body, and the static electric potential of a moving body. This corresponds exactly to the two components

Ψ_a and Ψ_b, which will be called respectively the *stepping component* and the *movement component*. By extension, ψ_a and ψ_b bear the same designation.

5. APPLYING THE MODEL

After having derived a forward model, which enables us to predict sensor values based on a person's location and body electric potential, we now invert the model. The inverse model allows us to analyze sensor data and estimate a person's location. Based on the localization, we reconstruct the person's change in body electric potential used for identification. Being aware of the simplifications introduced in our model, we also gain a better understanding of possible effects on localization and identification performance.

5.1 Localization

As described in the forward model, each raw sensor signal $v_\mathrm{S}(t)$ consists of two components. Contrary to the movement component $\psi_\mathrm{b}(t)$, the stepping component $\psi_\mathrm{a}(t)$ is very distinct and enables us to estimate the location of a person. However, the two components of (9) are superposed in the raw sensor signal and can hardly be separated in the time domain. By band-pass filtering $v_\mathrm{S}(t)$ around a realistic stepping frequency of 1 to 2.5 Hz [43], we obtain the *estimated stepping component* $\hat{\psi}_\mathrm{a}$. Another simplification we introduce is that the filtering simply attenuates the fundamental of the real signal Ψ_a without distorting it. Thus, the estimated stepping component is

$$\hat{\psi}_\mathrm{a}(t) \approx GK\Psi_\mathrm{a}(t) = GKR_\mathrm{in}C_\mathrm{C}(t){v_\mathrm{B}}'(t) \;, \qquad (10)$$

with G a constant that represents the combined gain of the measurement and the processing filter at the stepping frequency.

We combine the output of several sensors to localize the person. A *sensor pair* with sensors S_i and S_j performs two independent electric field measurements. The parameters and signals specific to a sensor S_i will be noted in the following with the index i, e.g. $C_{\mathrm{C}i}$ is the coupling capacitance between the body and sensor S_i. The filtered output of a sensor S_i is

$$\hat{\psi}_{\mathrm{a}i}(t) \approx \frac{GK_iR_\mathrm{in}C_{\mathrm{C,max}}H^\alpha {v_\mathrm{B}}'(t)}{([x(t)-x_{\mathrm{S}i}]^2+[y(t)-y_{\mathrm{S}i}]^2+H^2)^{\alpha/2}} \;, \quad (11)$$

When detecting a peak in two sensor signals, we can compare the ratio between them, corrected with the calibration factors (assumed to be known) and take the α-th root. The ratio has the advantage of eliminating $C_{\mathrm{C,max}}$, which is difficult to estimate in general. Assuming that the EPS have the same characteristics, and that the signals are processed by the same filter, R_in and G are also eliminated. Lastly, ${v_\mathrm{B}}'(t)$ disappears in the ratio, and the obtained function is purely dependent on the position. The α-th root cancels the $1/d^\alpha$ proportionality of the electric field. We call the resulting function *estimated distance ratio*, and note it $\hat{\Delta}_{ij}$ for the sensor pair $(\mathrm{S}_i, \mathrm{S}_j)$:

$$\hat{\Delta}_{ij}(t) = \sqrt[\alpha]{\frac{K_j\hat{\psi}_{\mathrm{a}i}(t)}{K_i\hat{\psi}_{\mathrm{a}j}(t)}} \approx \Delta_{ij}(t) \;. \qquad (12)$$

The actual *distance ratio* Δ_{ij} is given by

$$\Delta_{ij}(t) = \sqrt{\frac{[x(t)-x_{\mathrm{S}j}]^2+[y(t)-y_{\mathrm{S}j}]^2+H^2}{[x(t)-x_{\mathrm{S}i}]^2+[y(t)-y_{\mathrm{S}i}]^2+H^2}} \;. \qquad (13)$$

The parameters of Δ_{ij} are the sensors' coordinates, which are known, the ceiling to head distance H and the distance exponent α, that can be estimated. There are two unknowns x and y with only one equation, and a single sensor pair is still not sufficient to find the person's coordinates.

Similarly to RF-based systems that use propagation models for trilateration [12], at least three estimated distance ratios such as (12) are needed to find the person's coordinates with no sign ambiguity. In a non-ideal case, the system of three or more equations must be optimized to find the coordinates that minimize the error, i.e. the person's estimated position.

Our basic installation consists of four sensors organized in a rectangular *sensor cell*, which provides four distance ratios. A larger area can be covered by installing more sensor cells. In that case, the first step of localization is to find in which cell the sum of signal amplitudes is the strongest. Optimizing the coordinates based on the distance ratios is then accomplished within this cell only.

5.2 Body Electric Potential Change

The information about a person's location enables us to inverse another step presented in the forward model (Section 4.2) in order to derive the change in the body electric potential. The change in body electric potential is a powerful modality, which will later help us to identify a person. Once the person's position has been estimated, the equation of the stepping component for an individual sensor (11) can be solved for the derivative of the body electric potential:

$${v_\mathrm{B}}'(t) \approx \hat{v}_\mathrm{B}'(t) = \frac{\hat{\psi}_{\mathrm{a}i}(t)d_i(t)^\alpha}{K_iA} \;, \qquad (14)$$

where $d_i(t)$ is the Euclidean distance between the person and sensor S_i, and

$$A = GR_\mathrm{in}C_{\mathrm{C,max}}H^\alpha \;. \qquad (15)$$

The individual estimates $\hat{v}_\mathrm{B}'(t)$ (14) are combined by taking the weighted average over all sensors. In the following evaluation, we compare combining the predictions based on distance and equal weights.

If a reference measurement of the body electric potential is available, the error between the estimated and the real ${v_\mathrm{B}}'$ can be used as a cost to find an optimized value for A. Without a measurement, A is set arbitrarily and scales linearly to the real body electric potential.

5.3 Identification

During our experiments, it became obvious that body electric potential changes are very distinct for different people when taking a step. Reasons can be seen in a number of properties related to a human being, in particular gait cadence, but also footwear, synthetic materials worn, or body height. These properties contribute to a characteristic charging and coupling behaviour.

In the following we use the term *step signature* for a window of reconstructed body electric potential change around a step. We experimentally determined a window size of 0.72 ms as suitable to not interfere with the following step.

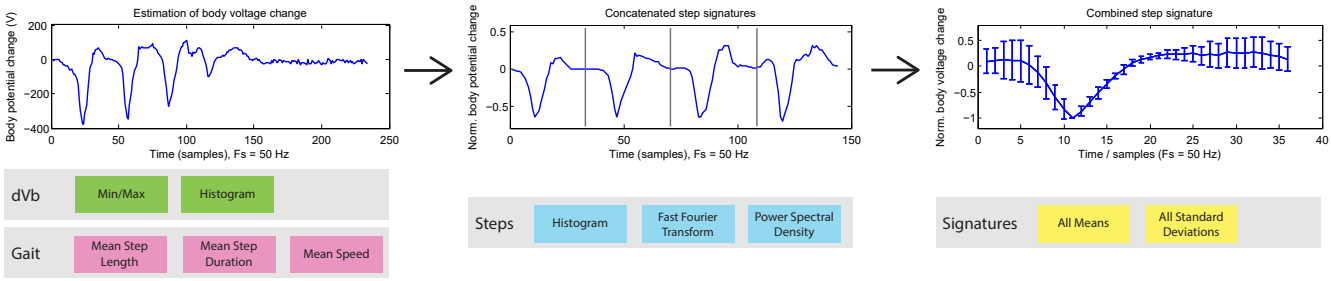

Figure 5: The feature extraction process for identification results in four feature sets: (1) *dVb* body electric potential, (2) *gait*-related, (3) a sequence of normalized *steps*, and (4) the combined and normalized step *signatures*.

Figure 5 shows an overview of the feature extraction process. Here, the negative peaks correspond to a user lifting the foot off the ground.

Although the step signatures may be of different amplitudes due to accumulation or decumulation of body charge, their shape remains quite constant. Therefore, the step signatures are normalized to a common scaling. In order to retrieve the frequency characteristics of all step signatures, we multiply each step signature by a Hamming window and concatenate them into one time-series, shown in the middle diagram of Figure 5. Based on this concatenated series of steps, we compute the Fast Fourier Transform (FFT), the Power Spectral Density (PSD), and a histogram.

The third diagram in Figure 5 depicts an overlay of all step signatures. We compute the mean step signature, as well as the standard deviation. All samples from both means and standard deviations are used as features. Based on the estimated electric potential and the localization, we also extract a few features that are typical in gait analysis [6]. We compute the mean step length and mean step duration to determine the gait cadence. Due to the fixed model parameter H (head to ceiling height), we currently do not take features like up- and down displacement into account.

6. EVALUATION

To evaluate Platypus, we collected a dataset in a controlled setting. The dataset comprises sensor measurements and a ground truth for localization and identification. We also recorded the human body electric potential to complete our dataset.

6.1 Test Setup and Participants

The data was collected in a room at Fraunhofer IGD (Darmstadt, Germany). The test room was approximately 16 m^2, with a metallic false ceiling 2.62 m high and a bare concrete floor. A sensor array of 2.5 m long by 2 m wide was installed on the ceiling. The array consisted of two rectangular sensor cells (i.e. six sensors), with each sensor at least 50 cm away from any wall. Markings on the floor materialized the limits of the covered area, the cell centers (for calibration) and start/stop points for the participants (Figure 6).

Thirty participants, all researchers and students at Fraunhofer IGD and TU Darmstadt, were involved in the experiment. The sample was predominantly male (three females), young (min. 16, max. 36, mean 28 years old) and tall (min. 1.60 m, max. 1.92 m, mean 1.79 m). All participants were asked to wear closed casual shoes for the experiment to minimize the effect of different types of footwear.

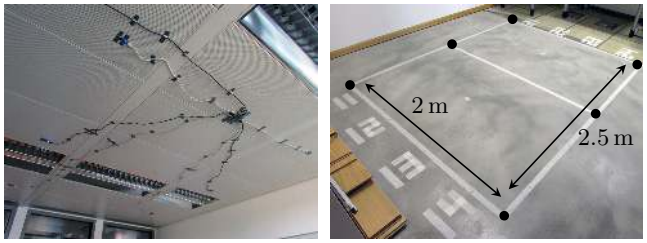

Figure 6: Setup of the model evaluation experiment. Left: six ceiling-mounted sensors arranged at the corners of two rectangular cells, and acquisition board. Right: marks on the floor defining the two sensor cells and the start/end locations of the walking paths. The sensors are located vertically above the sensor cells' corners, marked by black dots.

The participants were asked to walk on specific paths in the area covered the sensor array. For the position ground truth, we used a Kinect V2 [40]. Prior evaluation [62] has shown that this device has an accuracy in the range 1 mm to 10 mm, which is sufficient for evaluating our system. Ground truth for body electric potential was acquired using a high-impedance volt meter (model 820, Trek Inc.), connected to one wrist with a conductive strap.

6.2 Experimental Factors

Possible experimental factors were derived from the physical room situation, the participants' properties, the data processing scheme, and pre-tests of the system. The factors that depend on the physical situation are (1) room properties (flooring and ceiling material, ceiling height), (2) proximity of the sensors to room walls, and (3) presence of large grounded objects in the room. The participants' properties include (4) height, weight, footwear, and (5) walking speed. Data processing factors include (6) calibration constants K, (7) electric field distance exponent α and the (8) head to sensor distance H. This distance H is assumed as data processing factor, since it is not feasible to measure or estimate the body height of a person in the intended applications.

Room properties (1) and (2) are fixed for each room and installation, they are also assumed fixed in this first experiment. The presence of grounded objects is systematically varied with a grounded metal cart (1 m high, 1.2 m long and 0.5 m wide) placed in a corner of the localization area in half of all experimental runs. The properties of the partic-

ipants (4) are generally random and are not systematically varied in the experiment. Walking speed (5) is included as a nominal factor, asking participants to walk normally or slowly.

Two data processing factors were varied in the experiment, namely K and α. The calibration constants K used for estimating the distance ratio in (12) were either from an individual calibration for each test person or taken from a standard calibration performed by the second author. Pretests showed that $\alpha \approx 2.5$ could be a better choice than the theoretical $\alpha = 2$ as a value for the electric field distance exponent. This factor was evaluated on three levels. Head-to-ceiling-distance H showed no effect in the pre-tests. Therefore, H was calculated with the ceiling height using an average statue of 1.72 m [55].

This led to a $2 \times 2 \times 2 \times 3$ full factorial design with the factors walking speed, presence of grounded object, type of calibration (individual or standard) and the value of α. Only (speed $\times$ object) treatments needed an actual experiment, since all data processing factors could be varied in the calculations afterwards. Four repetitions per test person (i.e. 16 trajectories) were conducted.

For each participant, a series of eight trajectories with random start and stop points (see Fig. 6) and random speeds was drawn. The speeds were picked without replacement from a set of four "normal" and four "slow", to get a random order of speeds but always four normal walks and four slow ones. A similar series of eight start/stop/speed sets was picked for the tests with the grounded object present (eliminating the stop point 21, which was blocked by the object). Additionally, a calibration routine (100 steps in each cell) was performed by participants, to look at the effect of using individual calibration constants K rather than a system-wide calibration. The experiment lasted about 20 min per person and the results were analysed with SPSS version 22.

6.3 Localization Results

The localization error is calculated for detection i in the recording according to

$$\epsilon_i = \sqrt{(x_\mathrm{K}[k_i] - x_\mathrm{P}[k_i])^2 + (y_\mathrm{K}[k_i] - y_\mathrm{P}[k_i])^2}\,, \qquad (16)$$

where k_i are the discrete samples when signal peaks were detected, and the subscripts K and P indicate the true coordinates measured by the Kinect and the estimates given by the Platypus, respectively. The errors from all trajectories of a test person with the same treatment are pooled and the median is used as localization error measure for this treatment. This leads to 24 localization errors for each person, corresponding to the 24 treatments and 720 results in total.

We used linear regression to test the assumptions of negligible effects of test person height and weight as well as shoe size. Analysis shows a lack of significance for all participants' properties (height: $R^2 = 0.007$, $p = 0.657$; weight: $R^2 = 0.015$, $p = 0.525$; shoe size: $R^2 = 0.001$, $p = 0.902$). We therefore conclude that Platypus's localization errors are not sensitive to these factors.

Further analysis is based on a repeated-measures analysis of variance (ANOVA). From the total variation of this data set, 19.81 % can be attributed to the variations between participants. These variations cannot be described any further, but can be explained by individual properties of the participants not accounted for (e.g. clothing). The model above can explain 32.42 % of the variation, whereas

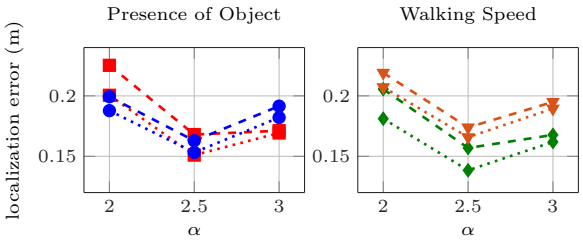

Figure 7: Interactions of α values on median localization error plots with object (left, square data points indicate object present, circles no object present) and walking speed (right, triangles indicate normal speed, diamonds slow speed). Calibration level is marked with dotted lines (standard) and dashed lines (individual).

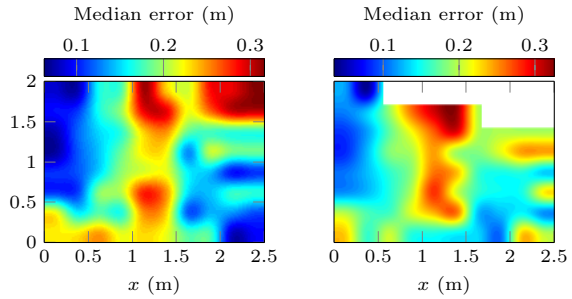

Figure 8: Median localization error over the covered area, without any object present (left) and with a grounded metallic cart in the top right corner (right). Because the cart was in the way, no trajectories entered the white zone. In both maps, the median error is largest at the border between the two cells ($x = 1.25$ m).

47.77 % are non-systematic variations. Given our ANOVA results, we derive the systematic variance and the reliability of this information.

A significant effect ($p < 0.001$) with medium size (i.e. accounting for about 10 % of the total variance) is found for the value of the electric field exponent α. As Figure 7 shows, the value $\alpha = 2.5$ gives much better results than the theoretical $\alpha = 2$. Further analysis showed that $\alpha = 2.5$ performs the best regardless of calibration level, walking speed, or the presence/absence of the grounded object. In the remaining we thus assume $\alpha = 2.5$.

On the other hand, although there is a significant effect ($p < 0.001$) of the calibration factor (with the standard calibration performing *better than individual*), the effect size is too small to have a relevant impact for the design of the system. We observed that calibration constants differ only in a very small range between participants, but in a much larger way depending on the positioning of the sensors, i.e. the room characteristics. Therefore, a standard calibration for each installation is sufficient for the use of Platypus, and future results refer to the standard calibration only.

The second largest effect ($p < 0.001$), albeit with small size (i.e. explaining about 1 % of the total variance), is observed for the walking speed factor. Slower walking speeds lead to smaller errors. We attribute this effect to a better performance of the separation of movement and stepping components by filtering, since the movement component has a lower frequency for slow movements. Due to the small ef-

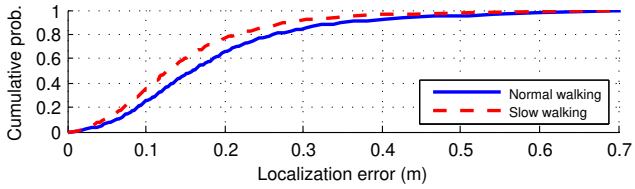

Figure 9: Cumulative distribution of localization error: The median error is 0.16 m for normal walking and 0.13 m for slow walking. 95 % of errors are under 0.36 m (slow walking) and 0.47 m (normal walking).

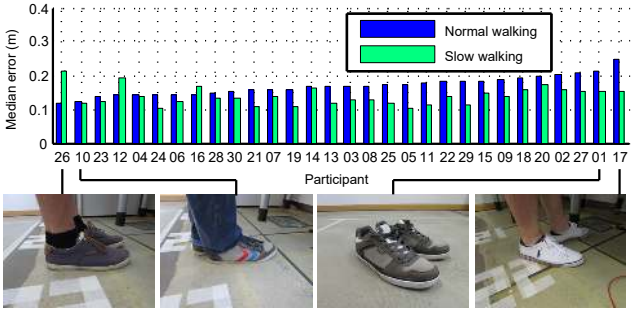

Figure 10: Localization median errors per user: the error shows no correlation with shoe size and body weight.

fect size, the error difference is in an acceptable range and we consider Platypus usable for both slow and normal walking speeds.

Overall, Platypus's localization error in this experimental configuration was found to have a median of 0.16 m for normal walking speed and 0.13 m for slow walking speeds (Figure 9). The ANOVA shows no significant effect of the metallic object on the localization error ($p = 0.640$, $\eta^2 = 0.0003$). We therefore conclude that Platypus is not adversely affected by static conductive objects. This is illustrated in Figure 8 which shows that locations close to the conducting object were not subject to high localization error. Figure 8 also illustrates that a 2 m by 1.25 m cell size of Platypus sensors leads to acceptable localization performance across the whole space. The user-dependent median localization errors are depicted in Figure 10. No correlation between shoe size and body weight with regard to the localization error could be observed.

6.4 Body Electric Potential Change

When a user's position, and thus the distance to a sensor, is known, it is possible to reconstruct the change in body electric potential using our model. To evaluate this, we compare the true change in body electric potential to the estimated change in body electric potential.

For a number of N discrete sampling points, we calculate the normalized root-mean-square error (NRMSE). The absolute RMSE can only provide limited insights, as the maximum and minimum body electric potential differ greatly from user to user:

$$\mathrm{NRMSE} = \frac{1}{\max v'_{\mathrm{B}} - \min v'_{\mathrm{B}}} \sqrt{\frac{\sum_{t=1}^{N} (\hat{v}'_{\mathrm{B,t}} - v'_{\mathrm{B,t}})^2}{N}}. \quad (17)$$

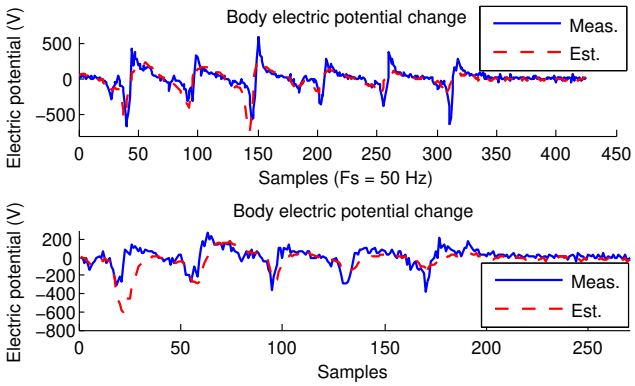

Figure 11: Top: Good estimate of body electric potential change with a NRMSE of 0.07. Bottom: Bad estimate with an NRMSE of 0.16.

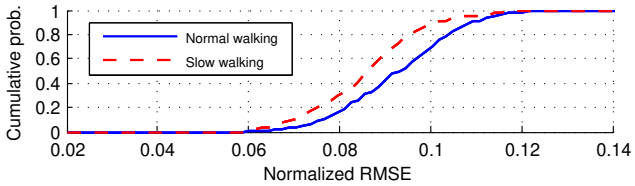

Figure 12: The body electric potential change estimation is most accurate for slow walking speeds. The NRMSE increases for normal walking speeds.

Figure 11 shows two examples of body electric potential change estimates and their ground truths. It can be seen that the estimates provide a good impression of the real change in body electric potential. However, as the stepping component $\hat{\psi}_{\mathrm{a}i}(t)$ is determined by band-pass filtering the sensor signals, some high-frequency features cannot be estimated. This results in smoother peaks for the estimated body electric potential change.

Fusing the estimates for body electric potential change can be achieved by summing up each sensor's prediction with equal weights. Using this technique, we achieve a mean NRMSE for slow walking of 0.085 ($\sigma = 0.012$), which shifts to 0.091 ($\sigma = 0.013$) for normal walking. Figure 12 shows the distribution of NRMSE for equal weighting. Assuming that the sensors closer to the person better estimate the change in body electric potential, we can also use the distances $d_i(t)^{\alpha}$ as weights. However, this results in a lower quality estimation, with a mean NRMSE of 0.098 ($\sigma = 0.018$) for slow walking, and 0.116 ($\sigma = 0.029$) for normal walking. The main reason can be seen in imprecise separation of stepping and movement component Ψ_{a} and Ψ_{b}. By applying equal weights, the influences of movement-related errors tend to cancel each other out as a person's distance to the sensors both increases and decreases.

6.5 Identification

To evaluate the identification performance based on location and body electric potential change we employ the feature sets introduced in 5.3. We use a standard SVM classifier (libSVM, RBF kernel, normalization) integrated in the WEKA framework [24]. The feature extraction is performed on a window comprising the whole trajectory of a partici-

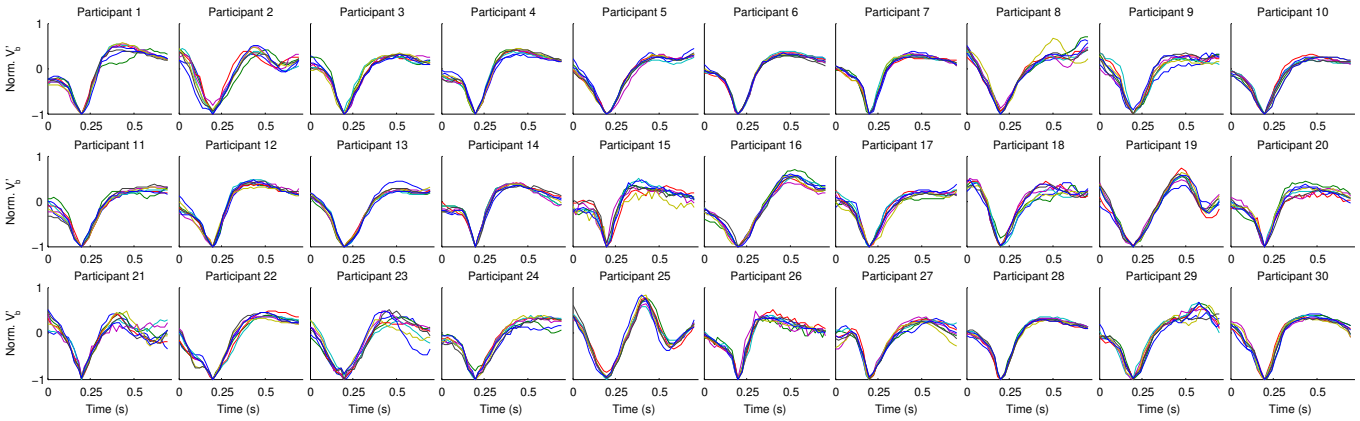

Figure 13: The estimated body electric potential changes when taking a step (step signatures) differ from user to user and represent a discriminative measure for classification. The amplitudes depend on the actually carried charge and require normalization.

Normal Walking	dVb	Gait	Steps	Signatures
dVb	49.3 %	56.2 %	65.6 %	**77.0 %**
Gait	-	29.0 %	48.8 %	65.6 %
Steps	-	-	47.2 %	70.1 %
Signatures	-	-	-	65.8 %
All sets	74.7 %			
Slow Walking	dVb	Gait	Steps	Signatures
dVb	55.1 %	64.2 %	**73.6 %**	69.6 %
Gait	-	35.1 %	59.2 %	63.6 %
Steps	-	-	51.1 %	63.6 %
Signatures	-	-	-	62.9 %
All sets	73.0 %			

Table 1: F-measures for identification of 30 participants walking with normal speeds (4-fold cross validation, 8 samples per participant).

pant (usually less than 5 s). Our identification is based on 30 participants, eight random trajectories with two movement speeds (240 windows for each speed). As a measure of classification performance, we apply the F-measure (or F1 score) which combines the measures of precision and recall.

First, we take a closer look on the four feature sets, containing information on body electric potential change (dVb), gait features (gait), steps (steps), and step signatures (signatures). We evaluate each single feature set and combinations between two feature sets. Each participant's dataset contains 2 x 8 randomized trajectories for slow and normal walking. The two walking speeds were first evaluated separately in a 4-fold cross validation, as listed in Table 1.

Combining all feature sets yields in an F-measure of 73.5% for slow walking and 74.7% for normal walking (average accuracy 75.0 %). It is conceivable that the feature set containing step signatures provides most discriminative data. Figure 13 depicts all extracted step signatures for the 30 participants. The most significant differences in the step signatures can certainly be seen in the rise and fall times of the signal (user 10, user 26). Also, the standard variance between consecutive steps differs greatly (user 21, user 7). Confusions in classification could be observed for very similar step signatures (user 15, user 1) or very irregular signatures (user 21).

The gait features provided least discriminative data. We believe that this can be attributed to the rather short trajectory, which did not allow the participants to move with a regular cadence. Also, the dataset contains people with very similar body height and physical condition, which leads to a very similar step pattern. The feature set comprising absolute change in body electric potential provided discriminative features and performed second best. A cross-validation between the data for each movement speed showed that the extracted features, especially the step signature, are inherently different. This leads to the conclusion that a user identification must be based on the natural movement pattern and does not generalize over multiple speeds.

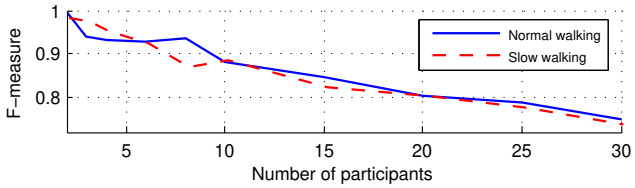

Figure 14: Identification accuracy compared to the number of people in the dataset.

In the following, we evaluate the influence of a different number of participants on the classification result. We conducted 10 repetitions on a 4-fold cross validation for a set of N randomly drawn participants. The results shown in Figure 14 indicate that two participants can be distinguished almost perfectly. The performance degrades with the number of people. Only slight differences in classification performance could be observed for walking slowly and normally.

7. CORRIDOR EXPERIMENT

We deployed Platypus in a corridor to evaluate a more realistic environment with less movement constraints. We recorded a dataset that contains sensor data and ground truth concerning walking four discrete paths along the corridor, as well as the participants' identities, covering multiple days. The questions we would like to answer with this experiment are whether participants can be reliably recognized even on different days and how different types of footwear influence the identification. We also evaluate whether Platypus is able to classify which path down the corridor was taken.

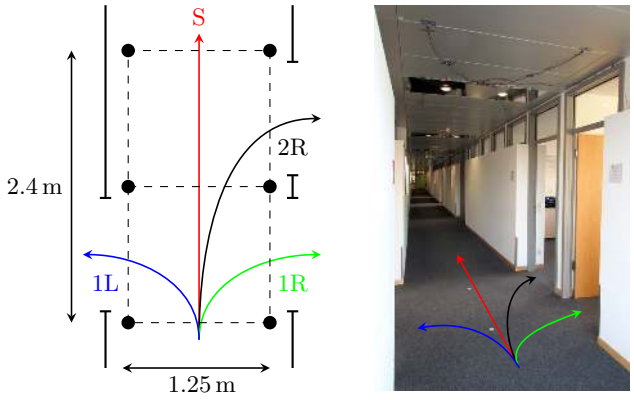

Figure 15: Left: Corridor experiment setup with six sensors (black circles) and four possible paths. Right: The deployment with sensors mounted to the ceiling.

7.1 Setup & Participants

We conducted this evaluation in a semi-controlled manner. Six sensors were installed on the ceiling of an office corridor with three doors (Figure 15). In contrast to the first experiment, a synthetic carpet covered the floor. We asked the participants to start walking about 2 m away from the sensing area, then to enter one of the three rooms or keep going through the corridor. To avoid hampering the participants' movements with a wrist strap and a cable, the body electric potential was not measured. Since the people went out of line of sight through doors, positioning by Kinect was not reliable for this test. Thus, the ground truth for localization was limited to discrete paths (end of the corridor or one of the three rooms).

For each participant, the experiment comprised four sessions. In the first session, the person walked eight times through the corridor and four times through each door, for a total of 20 measurements. The paths were taken in a random order, different for each session. The second session was similar to the first, with a second pair of shoes (all shoes were the participants' own). In the third and fourth sessions, we repeated the procedure of the two first sessions using the same shoes, but different clothes, on another day. The participants were not asked to choose any particular type of shoes, or to walk in any particular way.

We had 8 participants (6 male, 2 female), between 20 and 52 years old (average 32 years old). Similar to the first experiment, the participants were relatively tall (min. 1.67 m, max. 2 m, mean 1.79 m). All participants were researchers and students at Fraunhofer IGD and TU Darmstadt.

7.2 Persistence of Identification Features

One central aim of the experiment was to find out whether there are similarities in the features that could identify people independently of their footwear. The results are based on an SVM classifier as in the first evaluation (libSVM, RBF kernel, normalization).

To evaluate the feasibility of recognizing a user after a certain time, we asked the participants to perform the experiment on two days, with a gap of one to five days. We validated the data based on eight straight trajectories, using data from one day for training, and the other day for validation (and vice-versa). To evaluate the performance

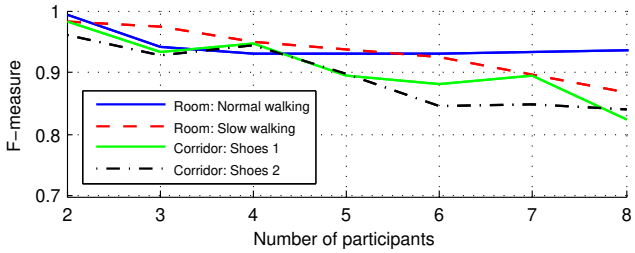

Figure 16: The classification performance of the corridor deployment evaluated on two different days compared to the controlled room experiment. Participants wore the same footwear on the two days.

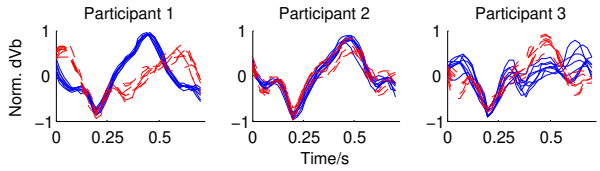

Figure 17: Most step signatures of participants changed when wearing different footwear. Few of them generated similar signatures, as shown in the middle plot.

depending on the number of people, we conducted 10 repetitions for a set of N random participants. The results are shown in Figure 16 and compared to data from the previous room experiment with the corridor experiment. For eight participants, we yield an average F-measure of 83.59 % (accuracy 83.6 %) in the corridor, which is less than the first room experiment for the same amount of participants (90.21 %). This can be attributed to the less controlled manner in which the experiment was carried out (no control over shoes, changed clothing, more freedom of movement).

Another question we investigated is whether it is possible to recognize a returning user with a different pair of shoes. Therefore, we combined data recorded on two days and used one pair of shoes for training, and the other for evaluation (and vice-versa). For eight users, the results indicate a poor average F-measure of just 26.15 %. We attribute this to differences in step signatures due to materials which influence contact charging, and different sole thicknesses which result in a different capacitive coupling to the floor (Figure 17).

For application developers, it is especially vital to know how many training samples are required to achieve a certain identification performance. For each number of training samples and number of people, we trained the classifier with 100 randomly drawn permutations containing straight

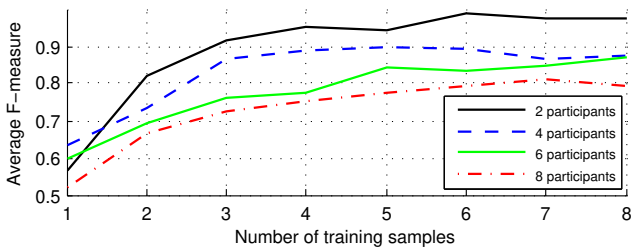

Figure 18: The identification performance stabilizes after 3-6 training samples of a 2.4 m walk.

	Recognized as			
	S	**1L**	**1R**	**2R**
S	244	3	9	0
1L	0	127	0	1
1R	0	4	119	5
2R	0	3	3	122

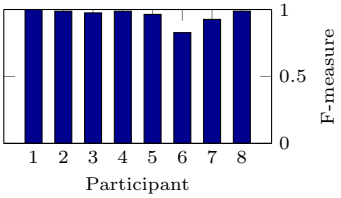

Figure 19: Left: confusion matrix for the trajectory classification. The four trajectories are noted as S (straight), 1L (first door, left of the corridor), 1R (first door, right) and 2R (second door, right). Right: average F-measure of path classification per participant.

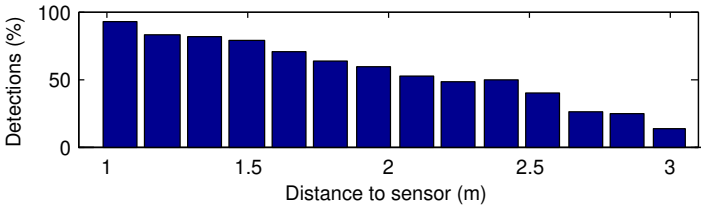

Figure 20: The rate of successful Platypus detections compared to distance, when a footstep occurs. The histogram starts at 1 m distance to account for head-to-ceiling height.

trajectories from day 1. We evaluated the trained classifier instances with all 8 straight trajectories recorded on day 2 (Figure 18). The results show that the classification performance stabilizes quickly for a small amount of users. Considering eight users, a stable performance is achieved after 5 - 6 training samples of a 2.4 m walk.

7.3 Trajectory Classification

Besides identification, we investigate how well Platypus recognizes one of the four possible paths taken within the corridor. We applied dynamic time warping (DTW) for classification [59], with the localization events as time series. As reference templates, we defined four mean paths based on all recorded trajectories.

Over all recordings, the classification accuracy reaches 95.6 %. The confusion matrix can be seen in Figure 19 (left). The F-measure by participant is shown in Figure 19 (right), and the average over all trajectories and all participants is 95.7 %. While the classification performance is almost perfect for many users, we observed a poor recognition accuracy for participant 6 (50 %) on one day and with one pair of shoes. This inaccuracy was not observed during the second day of measurement with the same shoes.

8. LIMITATIONS

Our experiments have shown that Platypus operates without the need for person-specific sensor calibration, and that it is independent of the user's height/weight/clothing as well as the presence or absence of grounded electrical objects in the environment. However, person-specific model training is still required, and identification of users depends on wearing the same footwear.

The experimental deployments are relatively dense (grid size from 1.2 m to 2 m) which is challenging when scaling to larger spaces. Figure 20 depicts the sensing range achieved using our current hardware and signal processing, and shows that the underlying electric field sensing does work at longer distances. In order to create more sparse deployments and lower the cost of Playtpus, future work can explore ways of increasing this range, for example by employing multiple analog frontends with different gain levels. This would also enable different topologies than grids - e.g. by arranging multiple sensors in a ceiling lamp.

Although smaller grounded objects do not affect the localization accuracy, we found that walls have a very strong coupling to users. This leads to an attenuated signal when person-to-wall distances are less than 30 cm, which could create blind spots in a deployed Platypus system near walls. A modified capacitive coupling model that not only includes the person-to-sensor coupling, but also the person-to-wall coupling, can potentially overcome this issue.

9. SUMMARY & FUTURE WORK

We introduced Platypus, a tag-free system to localize a person and to extract a signature pattern for identification. It is based on a novel use of electric field sensing to remotely infer a person's body electric potential changes. Our experiments have shown that using a 6-sensor array covering an area of 2 m by 2.5 m, Platypus can perform localization with a median error of 0.16 m while walking, and identification of 30 persons with an average accuracy of 75 % in a controlled setting. While the sensor density is high, the passive operation enables sensor designs with very low power consumption. Platypus incorporates a mathematical model which uses data from remote passive electric potential sensors to infer a human body electric potential, with a normalized root-mean-square error of 9.1 %. In a further, less constrained experiment, Platypus could identify 8 walking people with an average accuracy of 83.6 % using different days for training and testing. Depending on the number of users, Platypus's classification performance stabilizes after 3 - 6 training trajectories.

Some future work has already been described in the previous seciton. Other future work includes model refinements, most importantly the elimination of simplifications like stepping and movement component separation. We aim to analyse correlations between sensor signals that occur due to stepping, and are caused to a lesser extent by the movement component. This may lead to better localization and identification performance. Moreover, future model extensions include the localization and identification of multiple people, which would require distinguishing between multiple superposed signals. To avoid the installation of more sensors, we believe that our work towards identification can help separate the person-dependent signals.

We believe that remote passive sensing of electrical potential changes in the body is a promising technique that can be applied to other scenarios than we have so far addressed. Applications could include recognition of touch interactions with objects or other people in the environment, emergency situation recognition such as epileptic fits, as well as gait and gesture recognition.

Acknowledgements

We would like to thank Robert Prance and Daniel Roggen, University of Sussex, for initial explorations that inspired this work.

10. REFERENCES

[1] F. Adib, Z. Kabelac, D. Katabi, and R.C. Miller. 3D tracking via body radio reflections. In *Proceedings of the 11th USENIX Conference on Networked Systems Design and Implementation*, NSDI'14, pages 317–329, Berkeley, CA, USA, 2014. USENIX Association.

[2] H. Aly and M. Youssef. An analysis of device-free and device-based wifi-localization systems. *Int. J. Ambient Comput. Intell.*, 6(1):1–19, 2014.

[3] A.D. Aronoff, W.H. Boghosian, and H.A. Jenkinson. Electrostatic means for intrusion detection and ranging. Technical report, DTIC Document, 1965.

[4] A. Aydin, P.B. Stiffell, R.J. Prance, and H. Prance. A high sensitivity calibrated electric field meter based on the electric potential sensor. *Meas. Sci. Technol.*, 21, 2010.

[5] S.T. Beardsmore-Rust. *Remote applications of electric potential sensors in electrically unshielded environments*. PhD thesis, University of Sussex, 2010.

[6] C. BenAbdelkader, R. Cutler, and L. Davis. Person identification using automatic height and stride estimation. In *Pattern Recognition, 2002. Proceedings. 16th International Conference on*, volume 4, pages 377–380 vol.4, 2002.

[7] M.S. Brandstein and H.F. Silverman. A practical methodology for speech source localization with microphone arrays. *Computer Speech and Language*, 11(2):91–126, 1997.

[8] A. Bränzel, C. Holz, D. Hoffmann, D. Schmidt, M. Knaust, P. Lühne, R. Meusel, S. Richter, and P. Baudisch. Gravityspace: Tracking users and their poses in a smart room using a pressure-sensing floor. In *Proceedings of the SIGCHI Conference on Human Factors in Computing Systems*, CHI '13, pages 725–734, New York, NY, USA, 2013. ACM.

[9] A. Braun, H. Heggen, and R. Wichert. Capfloor - a flexible capacitive indoor localization system. In S. Chessa and S. Knauth, editors, *Evaluating AAL Systems Through Competitive Benchmarking. Indoor Localization and Tracking*, volume 309 of *Communications in Computer and Information Science*, pages 26–35. Springer Berlin Heidelberg, 2012.

[10] G.S.P. Castle. Contact charging between insulators. *Journal of Electrostatics*, 40/41:13–20, 1997.

[11] J. Chang, A.J. Kelly, and J.M. Crowley. *Handbook of Electrostatic Processes*. Marcel Dekker, Inc., 1995.

[12] K. Chintalapudi, A. Padmanabha Iyer, and V.N. Padmanabhan. Indoor localization without the pain. In *Proceedings of the Sixteenth Annual International Conference on Mobile Computing and Networking*, MobiCom '10, pages 173–184, New York, NY, USA, 2010. ACM.

[13] A.J. Clippingdale. *The sensing of spatial electrical potential*. PhD thesis, University of Sussex, 1993.

[14] G. Cohn, S. Gupta, T. Lee, D. Morris, J.R. Smith, M.S. Reynolds, D.S. Tan, and S.N. Patel. An ultra-low-power human body motion sensor using static electric field sensing. In *Proceedings of the 2012 ACM Conference on Ubiquitous Computing*, UbiComp '12, pages 99–102, New York, NY, USA, 2012. ACM.

[15] Gabe Cohn, Daniel Morris, Shwetak Patel, and Desney Tan. Humantenna: using the body as an antenna for real-time whole-body interaction. In *CHI '12*, pages 1901–1910, 2012.

[16] N. U. Czech-Damal, G. Dehnhardt, P. Manger, and W. Hanke. Passive electroreception in aquatic mammals. *Journal of Comparative Physiology A*, 199(6):555–563, 2013.

[17] T. Ficker. Electrification of human body by walking. *Journal of Electrostatics*, 64:10–16, 2006.

[18] S. Gabriel, R.W. Lau, and C. Gabriel. The dielectric properties of biological tissues: II. Measurements in the frequency range 10 Hz to 20 GHz. *Physics in Medicine and Biology*, 41(11):2251–2269, 1996.

[19] W. Gebrial, R. J. Prance, C.J. Harland, and T.D. Clark. Noninvasive imaging using an array of electric potential sensors. *Review of Scientific Instruments*, 77(6), 2006.

[20] T. Grosse-Puppendahl, Y. Berghoefer, A Braun, R. Wimmer, and A Kuijper. Opencapsense: A rapid prototyping toolkit for pervasive interaction using capacitive sensing. In *Pervasive Computing and Communications (PerCom), 2013 IEEE International Conference on*, pages 152–159, March 2013.

[21] T. Grosse-Puppendahl, A. Braun, F. Kamieth, and A. Kuijper. Swiss-Cheese Extended: An Object Recognition Method for Ubiquitous Interfaces based on Capacitive Proximity Sensing. In *CHI '13*, pages 1401–1410, 2013.

[22] Y. Guo and M. Hazas. Localising speech, footsteps and other sounds using resource-constrained devices. In *10th International Conference on Information Processing in Sensor Networks (IPSN)*, pages 330–341, 2011.

[23] Marian Haescher, Denys J. C. Matthies, Gerald Bieber, and Bodo Urban. Capwalk: A capacitive recognition of walking-based activities as a wearable assistive technology. In *Proceedings of the 8th ACM International Conference on PErvasive Technologies Related to Assistive Environments*, PETRA '15, pages 35:1–35:8, New York, NY, USA, 2015. ACM.

[24] M. Hall, E. Frank, G. Holmes, B. Pfahringer, P. Reutemann, and I.H. Witten. The weka data mining software: An update. *SIGKDD Explorations*, 11(1), 2009.

[25] C.J. Harland, T.D. Clark, and R.J. Prance. Electric potential probes - new directions in the remote sensing of the human body. *Measurement Science and Technology*, 13(2):163–169, 2002.

[26] D. Hauschildt and N. Kirchhof. Advances in thermal infrared localization: Challenges and solutions. In *2010 International Conference on Indoor Positioning and Indoor Navigation*, pages 1–8, 2010.

[27] K. Hidaka. Electric field and voltage measurement by using electro-optic sensor. In *Eleventh International Symposium on High Voltage Engineering*, volume 2, pages 1–14, 1999.

[28] T.W. Hnat, E. Griffiths, R. Dawson, and K. Whitehouse. Doorjamb: Unobtrusive room-level tracking of people in homes using doorway sensors. In *Proceedings of the 10th ACM Conference on Embedded Network Sensor Systems*, SenSys '12, pages 309–322, New York, NY, USA, 2012. ACM.

[29] P.M. Ireland. The role of changing contact in sliding triboelectrification. *Journal of Physics D: Applied Physics*, 41(2), 2008.

[30] C.D. Kidd, R. Orr, G.D. Abowd, C.G. Atkeson, I.A. Essa, B. MacIntyre, E. Mynatt, T.E. Starner, and W. Newstetter. The aware home: A living laboratory for ubiquitous computing research. In *Cooperative Buildings. Integrating Information, Organizations, and Architecture*, volume 1670 of *Lecture Notes in Computer Science*, pages 191–198. Springer Berlin Heidelberg, 1999.

[31] F. Kirchbuchner, T. Grosse-Puppendahl, M.R. Hastall, M. Distler, and A. Kuijper. Ambient intelligence from senior citizens' perspectives: Understanding privacy concerns, technology acceptance, and expectations. In *Ambient Intelligence*, volume 9425 of *Lecture Notes in Computer Science*, pages 48–59. Springer International Publishing, 2015.

[32] T. Kivimäki, T. Vuorela, P. Peltola, and J. Vanhala. A review on device-free passive indoor positioning methods. *International Journal of Smart Home*, 8(1):71–91, 2014.

[33] K. Kurita, R. Takizawa, and H. Kumon. Detection of human walking motion based on measurement system of current generated by electrostatic induction. In *ICCAS-SICE, 2009*, pages 5485–5488, 2009.

[34] G. Laput, C. Yang, R. Xiao, A. Sample, and C. Harrison. Em-sense: Touch recognition of uninstrumented, electrical and electromechanical objects. In *Proceedings of the 28th Annual ACM Symposium on User Interface Software & Technology*, UIST '15, pages 157–166, New York, NY, USA, 2015. ACM.

[35] H. Liu, H. Darabi, P. Banerjee, and J. Liu. Survey of wireless indoor positioning techniques and systems. *IEEE Transactions on Systems, Man, and Cybernetics, Part C: Applications and Reviews*, 37(6):1067–1080, 2007.

[36] J. Liu, Y. Wang, Y. Chen, J. Yang, X. Chen, and J. Cheng. Tracking vital signs during sleep leveraging off-the-shelf wifi. In *Proceedings of the 16th ACM International Symposium on Mobile Ad Hoc Networking and Computing*, pages 267–276. ACM, 2015.

[37] P. Llovera, P. Molinié, A. Soria, and A. Quijano. Measurements of electrostatic potentials and electric fields in some industrial applications: Basic principles. *Journal of Electrostatics*, 67(2/3):457–461, 2009.

[38] J. Lowell and A.C. Rose-Innes. Contact electrification. *Advances in Physics*, 29(6):947–1023, 1980.

[39] R. Mautz. Indoor positioning technologies. ETH Zurich, 2012. Habilitation thesis.

[40] Microsoft. Kinect for Windows features. http://www.microsoft.com/en-us/kinectforwindows/meetkinect/features.aspx (date accessed 2015-08-24).

[41] G. Monaci and A. Pandharipande. Indoor user zoning and tracking in passive infrared sensing systems. In *Proceedings of the 20th European Signal Processing Conference (EUSIPCO)*, pages 1089–1093, 2012.

[42] S. Narayana, R.V. Prasad, V.S. Rao, T.V. Prabhakar, S.S. Kowshik, and M.S. Iyer. PIR sensors: Characterization and novel localization technique. In *Proceedings of the 14th International Conference on Information Processing in Sensor Networks*, IPSN '15, pages 142–153, 2015.

[43] A. Pachi and T. Ji. Frequency and velocity of people walking. *The Structural Engineer*, 83(3):36–40, 2005.

[44] Plessey Semiconductors. EPIC sensor. http://www.plesseysemiconductors.com/epic-plessey-semiconductors.php (date accessed 2015-12-09).

[45] H. Prance, P. Watson, R.J. Prance, and S.T. Beardsmore-Rust. Position and movement sensing at metre standoff distances using ambient electric field. *Meas. Sci. Technol.*, 23, 2012.

[46] R. Prance and C. Harland. Electric potential sensor, July 2 2009. US Patent App. 12/374,359.

[47] Q. Pu, S. Gupta, S. Gollakota, and S. Patel. Whole-home gesture recognition using wireless signals. In *Proceedings of the 19th Annual International Conference on Mobile Computing & Networking*, MobiCom '13, pages 27–38, New York, NY, USA, 2013. ACM.

[48] T.S. Ralston, G.L. Charvat, and J.E. Peabody. Real-time through-wall imaging using an ultrawideband multiple-input multiple-output (mimo) phased array radar system. In *Phased Array Systems and Technology (ARRAY), 2010 IEEE International Symposium on*, pages 551–558, Oct 2010.

[49] J. Rekimoto and H. Wang. Sensing gamepad: Electrostatic potential sensing for enhancing entertainment oriented interactions. In *Extended Abstracts on Human Factors in Computing Systems*, pages 1457–1460, 2004.

[50] C.A. Rezende, R.F. Gouveia, M.A. da Silva, and F. Galembeck. Detection of charge distributions in insulator surfaces. *Journal of Physics: Condensed Matter*, 21(26), 2009.

[51] H. Rimminen. *Detection of human movement by near field imaging: development of a novel method and applications*. PhD thesis, Aalto University, School of Science and Technology, 2011.

[52] M. Shankar, J.B. Burchett, Q. Hao, B.D. Guenther, and D.J. Brady. Human-tracking systems using pyroelectric infrared detectors. *Optical Engineering*, 45(10):106401–106401, 2006.

[53] J.R. Smith. *Electric Field Imaging*. PhD thesis, Massachusetts Institute of Technology, 1999.

[54] R. Srinivasan, C. Chen, and D.J. Cook. Activity recognition using actigraph sensor. In *Proceedings of the Fourth Int. Workshop on Knowledge Discovery form Sensor Data (ACM SensorKDD'10), Washington, DC, July*, pages 25–28, 2010.

[55] Statistisches Bundesamt. Mikrozensus - Fragen zur Gesundheit - Körpermaße der Bevölkerung 2013 (in German), 2014.

[56] T. Teixeira, G. Dublon, and A. Savvides. A survey of human-sensing: Methods for detecting presence, count, location, track, and identity. Technical report, ENALAB, 2010.

[57] M. Valtonen, T. Vuorela, L. Kaila, and J. Vanhala. Capacitive indoor positioning and contact sensing for

activity recognition in smart homes. *J. Ambient Intell. Smart Environ.*, 4(4):305–334, 2012.

[58] G. Wang, Y. Zou, and K.and Ni L.M. Zhou, Z.and Wu. We can hear you with wi-fi! In *Proceedings of the 20th Annual International Conference on Mobile Computing and Networking*, MobiCom '14, pages 593–604, New York, NY, USA, 2014. ACM.

[59] Q. Wang. Dynamic time warping (dtw), 2014. http://mathworks.com/matlabcentral/fileexchange/43156 (date accessed: 2015/11/15).

[60] A. Williams, D. Ganesan, and A. Hanson. Aging in place: Fall detection and localization in a distributed smart camera network. In *Proceedings of the 15th ACM International Conference on Multimedia*, MM '07, pages 892–901, New York, NY, USA, 2007. ACM.

[61] J. Wilson and N. Patwari. See-through walls: Motion tracking using variance-based radio tomography networks. *Mobile Computing, IEEE Transactions on*, 10(5):612–621, May 2011.

[62] K. Woolford. Defining accuracy in the use of kinect v2 for exercise monitoring. In *Proceedings of the 2nd International Workshop on Movement and Computing*, pages 112–119. ACM, 2015.

[63] P. Wu and F. Li. The pyroelectric sensor based system: Human tracking and self-calibration scheme. In *2012 International Conference on Information Science and Technology (ICIST)*, pages 839–846, 2012.

[64] C. You, H. Kao, B. Ho, N. Chen, Y. Hsieh, P. Huang, and H. Chu. Thermalprobe: Exploring the use of thermal identification for per-user energy metering. In *Internet of Things (iThings), 2014 IEEE International Conference on*, pages 554–561, Sept 2014.

[65] X. Zhou, Q. Hao, and H. Fei. 1-bit walker recognition with distributed binary pyroelectric sensors. In *2010 IEEE Conference on Multisensor Fusion and Integration for Intelligent Systems (MFI)*, pages 168–173, 2010.